Tech Briefs

NATIONAL AERONAUTICS AND SPACE ADMINISTRATION

Technology Focus

Computers/Electronics

Software

Materials

Mechanics

Machinery/Automation

Manufacturing

Bio-Medical

Physical Sciences

Information Sciences

Books and Reports

INTRODUCTION

Tech Briefs are short announcements of innovations originating from research and development activities of the National Aeronautics and Space Administration. They emphasize information considered likely to be transferable across industrial, regional, or disciplinary lines and are issued to encourage commercial application.

Availability of NASA Tech Briefs and TSPs

Requests for individual Tech Briefs or for Technical Support Packages (TSPs) announced herein should be addressed to

National Technology Transfer Center

Telephone No. **(800) 678-6882** or via World Wide Web at **www2.nttc.edu/leads/**

Please reference the control numbers appearing at the end of each Tech Brief. Information on NASA's Commercial Technology Team, its documents, and services is also available at the same facility or on the World Wide Web at **www.nctn.hq.nasa.gov**.

Commercial Technology Offices and Patent Counsels are located at NASA field centers to provide technology-transfer access to industrial users. Inquiries can be made by contacting NASA field centers and program offices listed below.

NASA Field Centers and Program Offices

Ames Research Center
Carolina Blake
(650) 604-1754
cblake@mail.arc.nasa.gov

Dryden Flight Research Center
Jenny Baer-Riedhart
(661) 276-3689
jenny.baer-riedhart@dfrc.nasa.gov

Goddard Space Flight Center
Nona Cheeks
(301) 286-5810
Nona.K.Cheeks.1@gsfc.nasa.gov

Jet Propulsion Laboratory
Art Murphy, Jr.
(818) 354-3480
arthur.j.murphy-jr@jpl.nasa.gov

Johnson Space Center
Charlene E. Gilbert
(281) 483-3809
commercialization@jsc.nasa.gov

Kennedy Space Center
Jim Aliberti
(321) 867-6224
Jim.Aliberti-1@ksc.nasa.gov

Langley Research Center
Sam Morello
(757) 864-6005
s.a.morello@larc.nasa.gov

John H. Glenn Research Center at Lewis Field
Larry Viterna
(216) 433-3484
cto@grc.nasa.gov

Marshall Space Flight Center
Vernotto McMillan
(256) 544-2615
vernotto.mcmillan@msfc.nasa.gov

Stennis Space Center
Robert Bruce
(228) 688-1929
robert.c.bruce@nasa.gov

NASA Program Offices

At NASA Headquarters there are seven major program offices that develop and oversee technology projects of potential interest to industry:

Carl Ray
Small Business Innovation Research Program (SBIR) & Small Business Technology Transfer Program (STTR)
(202) 358-4652 or
cray@mail.hq.nasa.gov

Dr. Robert Norwood
Office of Commercial Technology (Code RW)
(202) 358-2320 or
rnorwood@mail.hq.nasa.gov

John Mankins
Office of Space Flight (Code MP)
(202) 358-4659 or
jmankins@mail.hq.nasa.gov

Terry Hertz
Office of Aero-Space Technology (Code RS)
(202) 358-4636 or
thertz@mail.hq.nasa.gov

Glen Mucklow
Office of Space Sciences (Code SM)
(202) 358-2235 or
gmucklow@mail.hq.nasa.gov

Roger Crouch
Office of Microgravity Science Applications (Code U)
(202) 358-0689 or
rcrouch@hq.nasa.gov

Granville Paules
Office of Mission to Planet Earth (Code Y)
(202) 358-0706 or
gpaules@mtpe.hq.nasa.gov

TECH BRIEFS

NATIONAL AERONAUTICS AND SPACE ADMINISTRATION

Technology Focus: Data Acquisition

Computer Program Recognizes Patterns in Time-Series Data

NASA's Jet Propulsion Laboratory, Pasadena, California

A computer program recognizes selected patterns in time-series data like digitized samples of seismic or electrophysiological signals. The program implements an artificial neural network (ANN) and a set of N clocks for the purpose of determining whether N or more instances of a certain waveform, W, occur within a given time interval, T. The ANN must be trained to recognize W in the incoming stream of data. The first time the ANN recognizes W, it sets clock 1 to count down from T to

zero; the second time it recognizes W, it sets clock 2 to count down from T to zero, and so forth through the Nth instance. On the $N + 1$st instance, the cycle is repeated, starting with clock 1. If any clock has not reached zero when it is reset, then N instances of W have been detected within time T, and the program so indicates. The program can readily be encoded in a field-programmable gate array or an application-specific integrated circuit that could be used, for example, to detect

electroencephalographic or electrocardiographic waveforms indicative of epileptic seizures or heart attacks, respectively.

*This program was written by Charles Hand of Caltech for **NASA's Jet Propulsion Laboratory**. Further information is contained in a TSP (see page 1).*

This software is available for commercial licensing. Please contact Don Hart of the California Institute of Technology at (818) 393-3425. Refer to NPO-30636.

Program for User-Friendly Management of Input and Output Data Sets

NASA's Jet Propulsion Laboratory, Pasadena, California

A computer program manages large, hierarchical sets of input and output (I/O) parameters (typically, sequences of alphanumeric data) involved in computational simulations in a variety of technological disciplines. This program represents sets of parameters as structures coded in object-oriented but otherwise standard American National Standards Institute C language. Each structure contains a group of I/O parameters that "make sense" as a unit in the simulation program with which this program is used. The addition of options and/or elements to sets of parameters amounts to the addition of

new elements to data structures. By association of child data generated in response to a particular user input, a hierarchical ordering of input parameters can be achieved. Associated with child data structures are the creation and description mechanisms within the parent data structures. Child data structures can spawn further child data structures. In this program, the creation and representation of a sequence of data structures is effected by one line of code that looks for children of a sequence of structures until there are no more children to be found. A linked list of structures is created dy-

namically and is completely represented in the data structures themselves. Such hierarchical data presentation can guide users through otherwise complex setup procedures and it can be integrated within a variety of graphical representations.

*This program was written by Gerhard Klimeck of Caltech for **NASA's Jet Propulsion Laboratory**. Further information is contained in a TSP (see page 1).*

This software is available for commercial licensing. Please contact Don Hart of the California Institute of Technology at (818) 393-3425. Refer to NPO-30835.

Noncoherent Tracking of a Source of a Data-Modulated Signal

Properties of the modulation would be exploited to determine direction-dependent phase differences.

Lyndon B. Johnson Space Center, Houston, Texas

A proposed tracking receiver system containing three suitably positioned antenna elements and special signal-processing equipment would determine the direction of incidence of a microwave signal containing spread-spectrum digital data modulation. If the system were

to contain two sets of antenna elements separated by a known baseline, it could determine the location of the transmitter as the intersection of the lines of incidence on the two antennas. Such systems could be used for diverse purposes in outer space and on Earth, including

tracking astronauts and small robotic spacecraft working outside a spacecraft or space station, and locating cellular telephones from which distress calls have been made. The principle of operation does not require the transmission of a special identifying or distress signal

by the cellular telephone or other transmitter to be tracked; instead, the system could utilize the data signal routinely sent by the transmitter, provided that the signal had the characteristics needed for processing as described below.

In its simplest form, the system would include three microstrip-patch antennas positioned to define an isosceles right triangle and a Cartesian coordinate system as depicted in Figure 1. The element at the origin of coordinates would be termed the reference element. The antenna elements on the x and y axes would both be separated from the reference element by a distance of half a wavelength at the carrier frequency of the signal to be tracked.
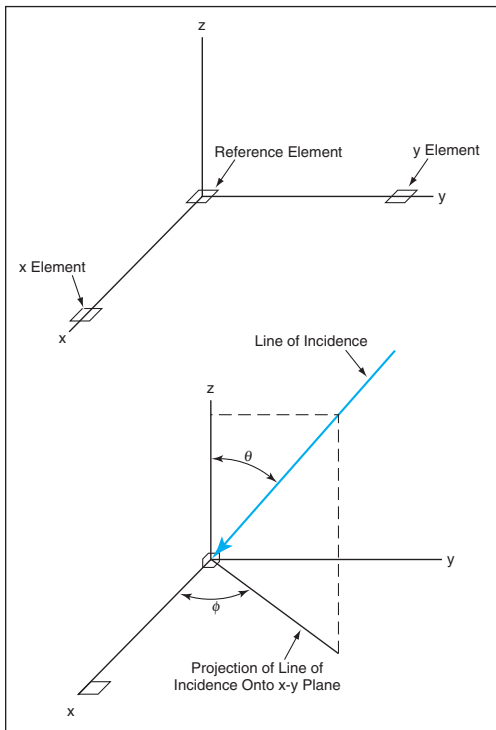

Figure 1. **Three Antenna Elements** would be positioned to define a coordinate system for measuring the angles, θ and φ, that specify the direction of incidence of a radio signal.

The basic equation for the phase of the incident signal can readily be manipulated to obtain the following equations for the colatitude (θ) and the azimuthal angle (φ) that specify the direction of incidence:

$$\theta = \arcsin\frac{\left(\Phi_1^2 + \Phi_2^2\right)^{1/2}}{\pi} \text{ and}$$
$$\phi = \arctan\left(\Phi_2/\Phi_1\right)$$

where Φ_1 is the difference between the signal phases at the x and reference antenna elements and Φ_2 is the corresponding phase difference for the y and reference elements. The tracking problem thus becomes one of determining Φ_1 and Φ_2. In the presence of multipath interference and noise, the tracking problem is complicated by the need to compute a separate pair of phase differences and the corresponding direction for each path.

In a transmitter to be tracked by a preferred version of the proposed system, the baseband data to be conveyed would be orthogonally coded, then spread into two channels by use of two independent pseudonoise (PN) codes. The resulting baseband signals in the two channels would be used to modulate the microwave carrier signal by quaternary phase-shift keying (QPSK).

In the receiver (see Figure 2), the intermediate-frequency (IF) signals from the three antenna elements would be digitized, then processed through quadrature down-converters, then processed through fingers (defined in the next sentence) and combiners, the use of which would simplify the hardware needed to track the multipath components. As used

here, "finger" signifies a time-multiplexed functional block that enables (at the expense of memory) the use of the same circuitry to track the signals arriving on multiple paths. Each finger would manage its own spreading-sequence timing and would perform its own multipath acquisition and tracking, despreading, and maximum-likelihood detection of orthogonal symbols. The combiners would provide the appropriate delays to align the symbols from the fingers for addition.

The multipath components would be resolved and the phase differences needed to compute the direction to the transmitter would be determined in a signal-processing scheme, the complexity of which admits of only a brief summary here: The scheme would involve noncoherent demodulation; that is, it would not rely on the generation, in the receiver, of a reference signal coherent with the phase of the carrier signal. Instead, it would rely on aligning the phases of local (receiver) PN code generators with the phases the transmitter PN code generators. The scheme would involve correlations of received modulation symbols with each and every one of the possible orthogonal symbols (of which there would be a total of 64 in the preferred version).
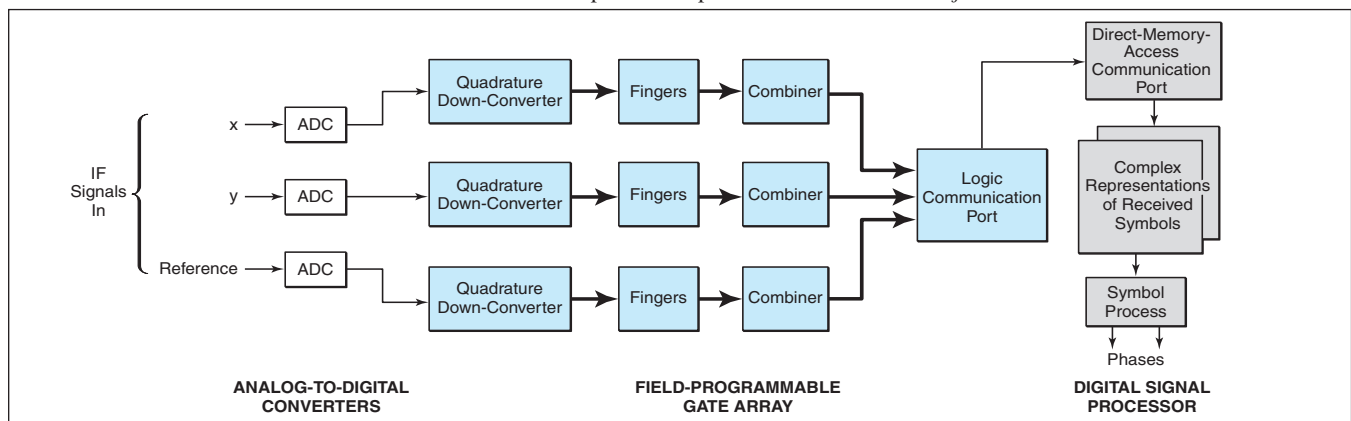
Figure 2. **Signals From the Antenna Elements Would Be Processed** to extract phase differences from modulation. The phase differences would be used to compute the angles θ and φ in Figure 1.

Software for Acquiring Image Data for PIV

John H. Glenn Research Center, Cleveland, Ohio

PIV Acquisition (PIVACQ) is a computer program for acquisition of data for particle-image velocimetry (PIV). In the PIV system for which PIVACQ was developed, small particles entrained in a flow are illuminated with a sheet of light from a pulsed laser. The illuminated region is monitored by a charge-coupled-device camera that operates in conjunction with a data-acquisition system that includes a frame grabber and a counter-timer board, both installed in a single computer. The camera operates in "frame-straddle" mode where a pair of images can be obtained closely spaced in time (on the order of microseconds). The frame grabber acquires image data from the camera and stores the data in the computer memory. The counter/timer board triggers the camera and synchronizes the pulsing of the laser with acquisition of data from the camera. PIVPROC coordinates all of these functions and provides a graphical user interface, through which the user can control the PIV data-acquisition system. PIVACQ enables the user to acquire a sequence of single-exposure images, display the images, process the images, and then save the images to the computer hard drive. PIVACQ works in conjunction with the PIVPROC program — described in prior *NASA Tech Briefs* articles — which processes the images of particles into the velocity field in the illuminated plane.

This program was written by Mark P. Wernet of **Glenn Research Center** *and H. M. Cheung of the University of Akron and Brian Kressler of Cornell University. Further information is contained in a TSP (see page 1).*

Inquiries concerning rights for the commercial use of this invention should be addressed to NASA Glenn Research Center, Commercial Technology Office, Attn: Steve Fedor, Mail Stop 4-8, 21000 Brookpark Road, Cleveland Ohio 44135. Refer to LEW-17373.

Detecting Edges in Images by Use of Fuzzy Reasoning
Human visual processing is partly imitated in order to harness some of its power.

John F. Kennedy Space Center, Florida

A method of processing digital image data to detect edges includes the use of fuzzy reasoning. The method is completely adaptive and does not require any advance knowledge of an image.

During initial processing of image data at a low level of abstraction, the nature of the data is indeterminate. Fuzzy reasoning is used in the present method because it affords an ability to construct useful abstractions from approximate, incomplete, and otherwise imperfect sets of data. Humans are able to make some sense of even unfamiliar objects that have imperfect high-level representations. It appears that to perceive unfamiliar objects or to perceive familiar objects in imperfect images, humans apply heuristic algorithms to understand the images.

Fuzzy reasoning is a suitable means of heuristic processing of incomplete and otherwise imperfect data. Most prior edge-detection methods require the selection of parameters (e.g., thresholds in gradient edge-detection algorithms) — a difficult task when little or nothing is known about an image in advance. Moreover, prior edge-detection methods based on mathematical models can detect only specific kinds of noticeable edges: For example, an optimal mathematical-model-based step edge detector can be ineffective in detecting ramp edges. Relative to methods that involve mathematical models and advance selec-

Original Image

Image After Processing by Prewit Edge Detector

Image After Processing by Sobel Edge Detector

Image After Processing by Fuzzy-Reasoning Edge Detector
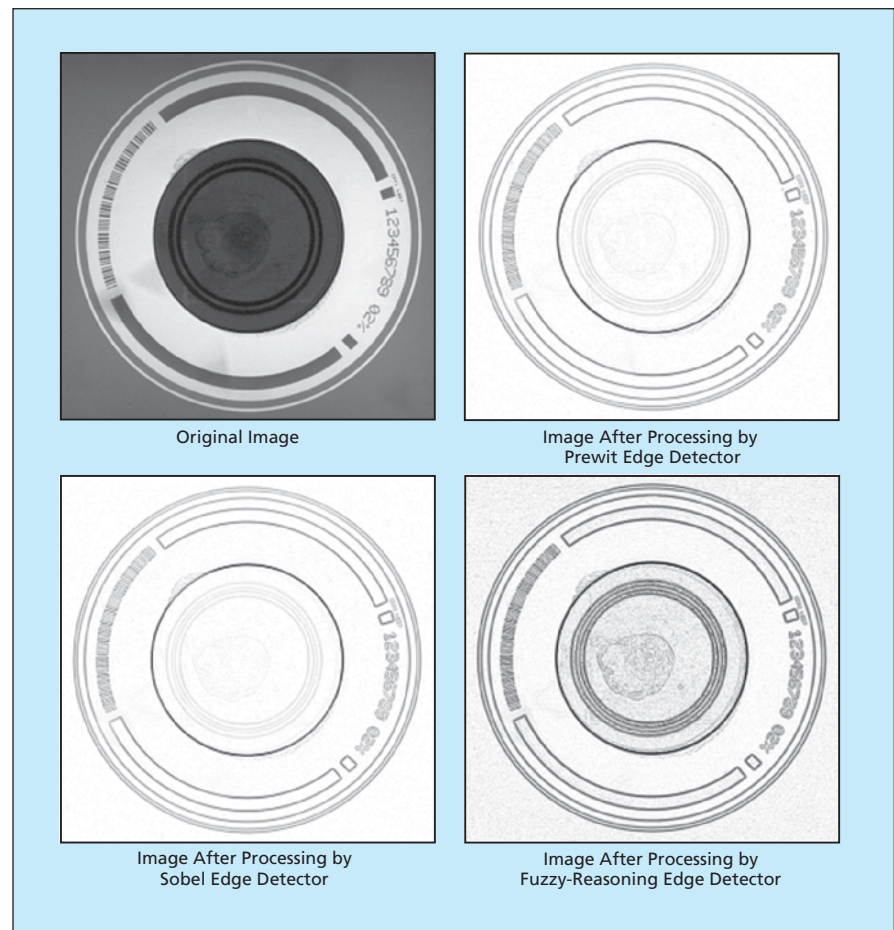
An **Image of a Compact Disk** was processed by a fuzzy-reasoning edge detector and by the Prewit and Sobel edge detectors.

tion of parameters, the present method and possibly other methods of processing image data in partial imitation of image processing in the human brain and eye offer greater flexibility and the potential for superior performance.

In the present method, a window of 3 by 3 pixels is scanned over the whole image. An optimal intensity gradient based on the central pixel is found through a heuristic analysis. A crisp cen-tral-pixel value is generated after a fuzzy membership function is evaluated by use of the optimal intensity gradient.

The method has been implemented in a C-language computer program. The method was tested by applying the program to an image of a compact disk. As shown in the figure, this method performed better at detecting edges than did computer programs that implemented two prior edge-detection methods known as the Sobel and Prewit methods. The program of the present method even detected a dark central spot containing narrow edges that the programs of the Sobel and Prewit methods did not detect at all.

A Timer for Synchronous Digital Systems

There is no discernible jitter in the output clock waveforms.

NASA's Jet Propulsion Laboratory, Pasadena, California

The Real-Time Interferometer Control Systems Testbed (RICST) timing board is a VersaModule Eurocard (VME)-based board that can generate up to 16 simultaneous, phase-locked timing signals at a rate defined by the user. It can also generate all seven VME interrupt requests (IRQs). The RICST timing board is suitable mainly for robotic, aerospace, and real-time applications.

Several circuit boards on the market are capable of generating periodic IRQs. Most are associated with Global Positioning System (GPS) receivers and Inter Range Instrumentation Group (IRIG) time-code generators, whereas this board uses either an internal VME clock or an externally generated clock signal to synchronize multiple components of the system. The primary advantage of this board is that there is no dis-

cernible jitter in the output clock waveforms because the signals are divided down from a high-frequency clock signal instead of being phase-locked from a lower frequency. The primary disadvantage to this board, relative to other periodic-IRQ-generating boards, is that it is more difficult to synchronize the system to wall clock time.

Real-time systems have traditionally utilized timers available on central-processing-unit (CPU) boards to generate IRQs. The RICST timing board combines that functionality with the ability to use the same signals to synchronize other parts of the system in which it is installed.

The RICST System Timing Board (see figure) includes 16 programmable digital output channels, seven of which can also be enabled to drive VME IRQ

lines 1 through 7. The signals in all 16 output channels are differential transistor/transistor-logic (TTL)-level square waves, at frequencies defined by the user, that are coupled out via ribbon-cable connectors mounted on a front panel. Optional hardware can be added to the board, so that six of the channels can generate analog outputs in addition to the standard digital outputs (e.g., sine waves instead of square waves). Most of the functions of the board are performed by a programmable logic device, with additional circuitry for controlling the VMEbus interface and output signals.
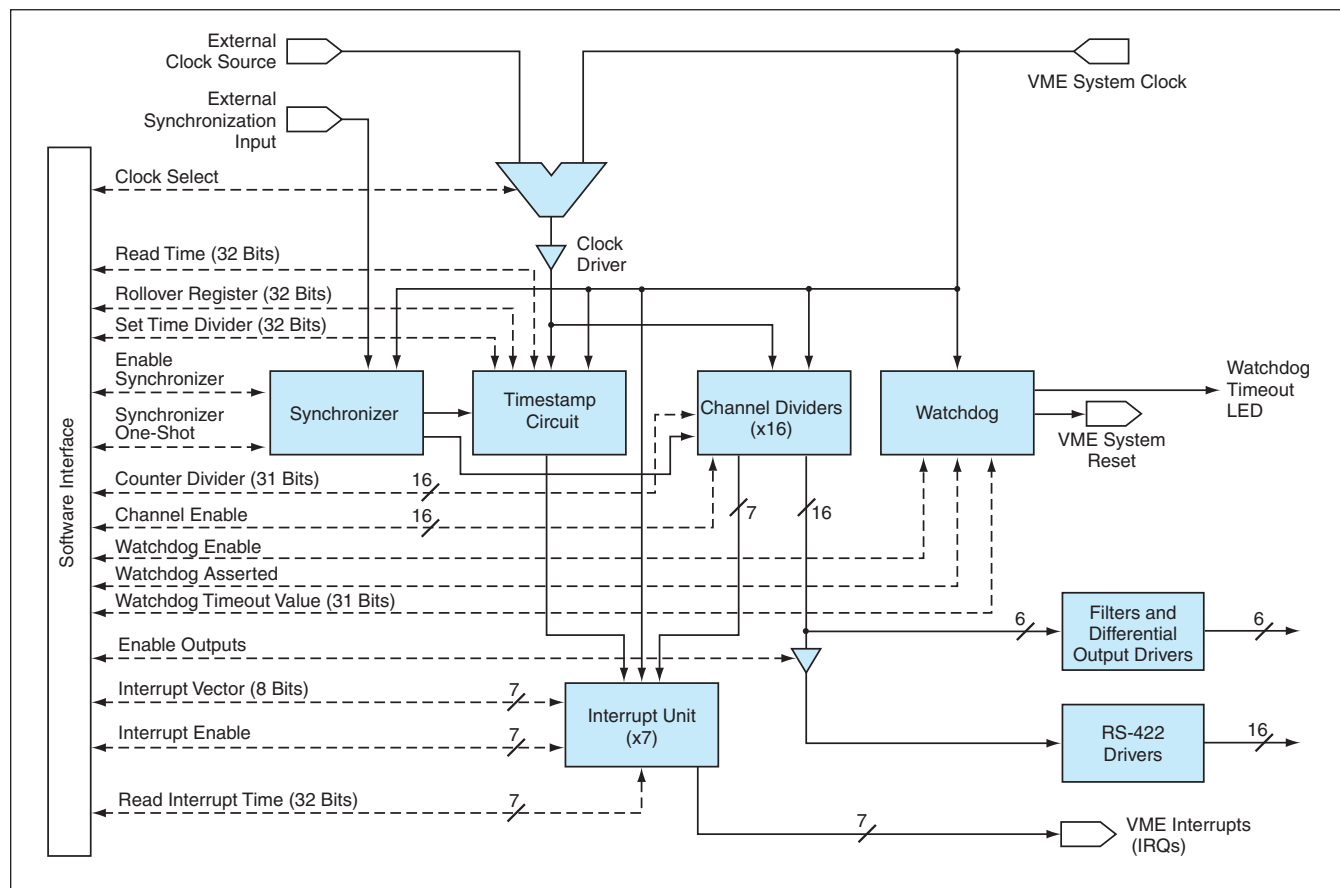
The **RICST Timing Board** generates clock signals and interrupt requests (IRQs). Optionally, it can be equipped to generate six analog outputs.

Prototype Parts of a Digital Beam-Forming Wide-Band Receiver

RSFQ circuits are used for digital processing at multigigahertz rates.

John H. Glenn Research Center, Cleveland, Ohio

Some prototype parts of a digital beam-forming (DBF) receiver that would operate at multigigahertz carrier frequencies have been developed. The beam-forming algorithm in a DBF receiver processes signals from multiple antenna elements with appropriate time delays and weighting factors chosen to enhance the reception of signals from a specific direction while suppressing signals from other directions. Such a receiver would be used in the directional reception of weak wideband signals — for example, spread-spectrum signals from a low-power transmitter on an Earth-orbiting spacecraft or other distant source.

The prototype parts include superconducting components on integrated-circuit chips, and a multichip module (MCM), within which the chips are to be packaged and connected via special inter-chip-communication circuits. The design and the underlying principle of operation are based on the use of the rapid single-flux quantum (RSFQ) family of logic circuits to obtain the required processing speed and signal-to-noise ratio. RSFQ circuits are superconducting circuits that exploit the Josephson effect. They are well suited for this application, having been proven to perform well in some circuits at frequencies above 100 GHz. In order to maintain the superconductivity needed for proper functioning of the RSFQ circuits, the MCM must be kept in a cryogenic environment during operation.

The DBF and cryogenic aspects of the receiver design make it possible to overcome the limitations of both (1) the inherently narrow-band nature of analog beam-forming circuits in which the differential time delays needed for beam
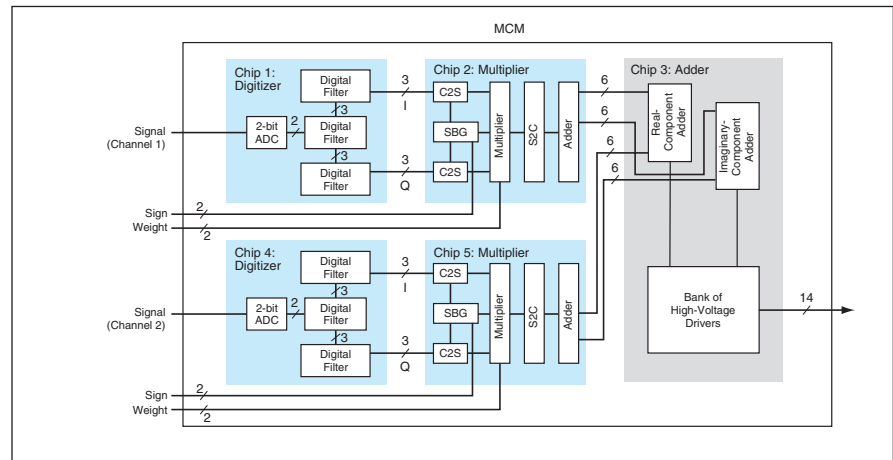
Five Chips in a Multichip Module would perform various digital signal-processing functions for a two-channel DBF receiver. The blocks marked "C2S," "S2C," and "SBG" perform conversions between complementary and signed-binary representations of numbers, as needed because the filter and adder circuits work best in complementary code, while the multipliers work best in signed binary code.

forming (including beam steering) are implemented via phase shifts and (2) the relatively slow speeds of room-temperature digital signal processors. A typical fully developed DBF receiver would have to contain more than two input-signal-processing channels for effectiveness in beam forming. For demonstrating feasibility at the present early stage of development, the prototype MCM is designed to accommodate two input-signal-processing channels.

The complete two-channel MCM would contain five chips: two analog-to-digital converter (ADC) chips, two multiplier chips, and an adder/driver chip (see figure). The ADC in each channel is designed to digitize the incoming signal to two bits at a sampling rate of 10 GS/s. The ADC chip includes a digital mixer and anti-aliasing filters that shift the signal frequency down to a bandwidth of

2.5 GHz and separate the signal into in-phase (I) and quadrature (Q) components. The multiplier in each channel is designed to introduce weighting and delay factors for steering. The adder portions of the adder/driver chip are designed to combine the I and Q signal components from the two channels. The driver portion is needed to amplify the outputs of the adders to avoid errors that could otherwise occur if one were to couple the low-level adder outputs directly to external room-temperature circuits.

This work was done by Steven B. Kaplan, Sergey V. Rylov, and Michael Pambianchi of HYPRES for **Glenn Research Center**.

Inquiries concerning rights for the commercial use of this invention should be addressed to NASA Glenn Research Center, Commercial Technology Office, Attn: Steve Fedor, Mail Stop 4–8, 21000 Brookpark Road, Cleveland, Ohio 44135. Refer to LEW-16935.

High-Voltage Droplet Dispenser

Individual droplets are released on command.

John H. Glenn Research Center, Cleveland, Ohio

An apparatus that is extremely effective in dispensing a wide range of droplets has been developed. This droplet dispenser is unique in that it utilizes a droplet bias voltage, as well as an ionization pulse, to release a droplet. Apparatuses that de-

ploy individual droplets have been used in many applications, including, notably, study of combustion of liquid fuels. Experiments on isolated droplets are useful in that they enable the study of droplet phenomena under well-controlled and

simplified conditions.

In this apparatus, a syringe dispenses a known value of liquid, which emerges from, and hangs onto, the outer end of a flat-tipped, stainless steel needle. Somewhat below the needle tip and

droplet is a ring electrode. A bias high voltage, followed by a high-voltage pulse, is applied so as to attract the droplet sufficiently to pull it off the needle. The voltages are such that the droplet and needle are negatively charged and the ring electrode is positively charged.

The droplet-dispenser circuit (see figure) includes power supply PS2, which energizes DC-to-DC converter PS4 to produce the bias voltage. A bias voltage of the order of 3 kV has been found to be effective. PS4 charges capacitor C2 through current-limiting resistor R9. Bleed resistor R8 discharges C2 for safety when the circuit is not in use. Diodes D5 and D6 protect PS4 from inductive voltage spikes. The droplet is charged via steering diode D4 and current-limiting resistor R7.

Power supply PS1 energizes DC-to-DC converter PS3 to charge capacitor C1 via current-limiting resistor R1. Charging C1 to 100 volts has been found to be effective. Bleeder resistor R2 discharges C1 for safety when the circuit is not in use. Silicon controlled rectifier SCR1 conducts when push-button switch S1 is closed momentarily, producing a microsecond pulse in the primary winding of transformer T1. Diodes D1 and D2 protect SCR1 from inductive spikes. When C1 has been charged to 100 V, a pulse of 12 kV is
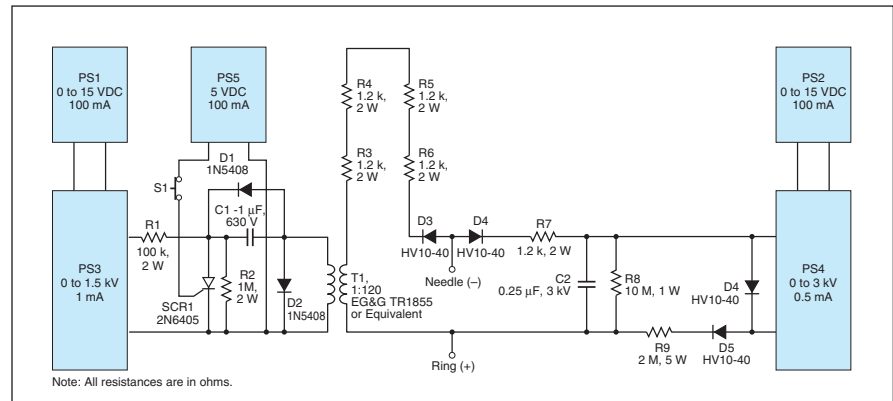
This **Electronic Circuit** of the high-voltage droplet dispenser generates a steady high bias voltage, upon which it superimposes a high-voltage pulse to release a droplet.

produced at the secondary winding of T1; however, the circuit is capable of generating a pulse of as much as 40 kV. The pulse provides ionization energy to the droplet via steering diode D3 and current-limiting resistors R3, R4, R5, and R6. This energy causes the release of the droplet. The four current-limiting resistors (instead of only one resistor with four times the resistance of one of them) are used here to enable this part of the circuit to withstand the high-voltage pulse.

Before the circuit is turned on, PS1 and PS2 are set to the minimum voltage levels. Then they are turned on along with PS5. Next, PS1 and PS2 are set to

the desired voltage levels. Finally, S1 is closed momentarily to release the droplet. The circuit as described here was designed for manual control, but is readily adaptable to control by a microprocessor.

This work was done by Dennis J. Eichenberg of **Glenn Research Center.** *Further information is contained in a TSP (see page 1).*

Inquiries concerning rights for the commercial use of this invention should be addressed to NASA Glenn Research Center, Commercial Technology Office, Attn: Steve Fedor, Mail Stop 4–8, 21000 Brookpark Road, Cleveland, Ohio 44135. Refer to LEW-17190.

Network Extender for MIL-STD-1553 Bus

Long-distance communications and equipment tests can be effected through a single multicoupled source.

Lyndon B. Johnson Space Center, Houston, Texas

An extender system for MIL-STD-1553 buses transparently couples bus components at multiple developer sites. The bus network extender is a relatively inexpensive system that minimizes the time and cost of integration of avionic systems by providing a convenient mechanism for early testing without the need to transport the usual test equipment and personnel to an integration facility. This bus network extender can thus alleviate overloading of the test facility while enabling the detection of interface problems that can occur during the integration of avionic systems. With this bus extender in place, developers can correct and adjust their own hardware and software before products leave a development site. Currently resident at Johnson

Space Center, the bus network extender is used to test the functionality of equipment that, although remotely located, is connected through a MIL-STD-1553 bus. Inasmuch as the standard bus protocol for avionic equipment is that of MIL-STD-1553, companies that supply MIL-STD-1553-compliant equipment to government or industry and that need long-distance communication support might benefit from this network bus extender.

The state of the art does not provide a multicoupler source for this purpose. Instead, the standard used by the military serves merely as an interface between a main computer in some device or aircraft and the subsystems of that device or aircraft — for example, a subsystem that controls wing flaps or ailerons.

Unfortunately, the transmission distance of a state-of-the-art MIL-STD-1553 system is limited to 400 ft (122 m). The bus network extender eliminates this distance restriction by enabling the integrated testing of subsystems that are located remotely from each other, without having to physically unite those subsystems. Interlinking by use of the bus network extender is applicable to 90 percent of all required testing for the military; hence, it offers the potential for savings in cost and time. There is also potential for commercial applications in simulation and training and in the development of real-time systems.

The bus network extender enables long-distance communications by use of specified media and compliant equipment, while conforming to all rel-

evant MIL-STD-1553 specifications, including those that pertain to response times and data formats. The bus network extender can also insert simulated or table-driven data addressed to any bus controller (BC) or remote-terminal (RT)/support-area (SA) network combination.

In a system under test, subsystems connected at a local site are connected to the bus network extender. After the connection is made, the output of a remote bus controller mimics the activity of the bus controller at the local site and can be configured to operate with multiple remote sites. The entire bus network is then controlled by a workstation coupled at the local site. The configuration of the bus network extender is controlled by a single text file that is created by the user and that can be modified at the local site.

In order to extend a network, the bus network extender effects a logical sequence of events. The BC (either simulated or hardware in the loop) first sends a MIL-STD-1553 message to the RT. The RT passes the message to a central processing unit (CPU). A master CPU reads the message and transmits an Ethernet (or equivalent) MIL-STD-1553 message to a slave CPU, which receives the message and begins building a MIL-STD-1553 BC message chain. The slave CPU then sends the MIL-STD-1553 message to the RT via BC hardware, a response to the message is received by the BC hardware, and the CPU is notified. After notification, a slave CPU returns the MIL-STD-1553 message response to the master CPU over the Internet. If the message is a "transmit" message, the master CPU fills the destination RT data buffer with response data. Finally, new data become available to the hardware-in-the-loop or simulated BC.

The bus network extender also provides the following:
- An RT/SA address can be mapped to a different RT/SA on the remote RT to avoid having to change jumpers or reprogram an address.
- The system can be set to respond to some SAs by simulating other SAs. This capability enables testing even when some sensors or devices on a remote unit under test are unavailable.
- Multiple MIL-STD-1553 buses can operate simultaneously.
- Common configuration files can be used to control and document the interfaces to the bus-network-extender interfaces.
- Responses to MIL-STD-1553 messages can be generated in real time.
- It is possible to perform byte swapping for computers or firmware controllers that are based on different processor architectures.

Performance depends on the type of communication channel used to connect local and remote sites. In a compromise, commands are buffered by the bus network extender and appear, at least to the BC, to satisfy response-time requirements. However, data supplied by the bus network extender to the BC are transmitted from one or more frame times in the past. The system thus operates correctly with respect to protocol and timing but is subject to a delay in data content ranging from tens of milliseconds to seconds. Such delays result from finite signal-propagation speed and are unavoidable. Notwithstanding such delays, the bus network extender is well suited for protocol and interface integration testing, even on slower links. On faster links, some systems equipped with the extender can cycle MIL-STD-1553 frames at full speed, subject to only inevitable data delays. Some systems equipped with bus network extenders may seem to operate in real time on high-speed links.

The bus network extender is equipped with utility software that, upon command, displays the status of all BCs, remote transmission queues, and RT message queues. The software also provides a configuration file for all connected systems to provide error-free configuration at all locations, a configuration file that contains an entire system interface control document, and an input file that performs extensive error checking. Since slave BCs are configured automatically, remote configuration data are totally eliminated when remote simulations are not required. Should a slave network server be unreachable, the extender attempts to reestablish network connections automatically while maintaining adherence to real-time-response requirements for all MIL-STD-1553 messages.

MMIC HEMT Power Amplifier for 140 to 170 GHz

Circuits like this one could be useful in radiometers for probing the atmosphere.

NASA's Jet Propulsion Laboratory, Pasadena, California

Figure 1 shows a three-stage monolithic microwave integrated circuit (MMIC) power amplifier that features high-electron-mobility transistors (HEMTs) as gain elements. This amplifier is designed to operate in the frequency range of 140 to 170 GHz, which contains spectral lines of several atmospheric molecular species plus subharmonics of other such spectral lines. Hence, this amplifier could serve as a prototype of amplifiers to be incorporated into heterodyne radiometers used in atmospheric science. The original intended purpose served by this amplifier is to boost the signal generated by a previously developed 164-GHz MMIC HEMT doubler [which was described in "164-GHz MMIC HEMT Frequency Doubler" (NPO-21197), *NASA Tech Briefs*, Vol. 27, No. 9 (September 2003), page 48.] and drive a 164-to-328-GHz doubler to provide a few milliwatts of power at 328 GHz.

The first two stages of the amplifier contain one HEMT each; the third (output) stage contains two HEMTs to maximize output power. Each HEMT is characterized by gate-periphery dimensions of 4 by 37 μm. Grounded coplanar waveguides are used as impedance-matching input, output, and interstage-coupling transmission lines.

The small-signal *S* parameters and the output power (for an input power of about 5 dBm) of this amplifier were measured as functions of frequency. For the small-signal gain measurements, the amplifier circuit was biased at a drain potential of 2.5 V, drain current of 240 mA, and gate potential of 0 V. As shown in
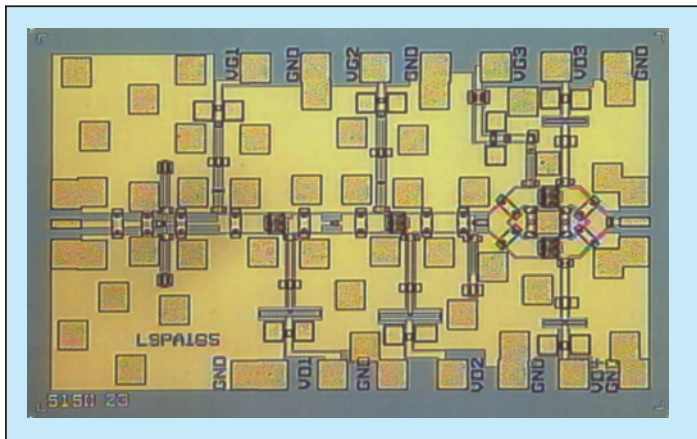
Figure 1. This **Three-Stage MMIC HEMT Amplifier** occupies a chip area with dimensions of 1.1 by 1.9 mm.

Figure 2. The **Small-Signal *S* Parameters and Power Output** of the amplifier were measured over its design frequency range.

the upper part of Figure 2, the small-signal gain (S_{21}), was found to be >10 dB from 144 to 170 GHz, while input and output return losses (S_{11} and S_{22}) are both approximately 10 dB at 165 GHz.

For the power measurements, the amplifier circuit was biased at a drain potential of 2.1 V, a drain current of 250 mA, and gate potential of 0 V (these biases were chosen to optimize the output power). As shown in the lower part of Figure 2, the output power ranged from a low of about 11.8 dBm (≈15 mW) to a high of about 14 dBm (≈25 mW). The peak power output of about 14 dBm was achieved at 150 GHz at an input power of 6.3 mW, yielding a large-signal gain of slightly less than 8 dBm.

This work was done by Lorene Samoska of **NASA's Jet Propulsion Laboratory**, *and Vesna Radisic, Catherine Ngo, Paul Janke, Ming Hu, and Miro Micovic of HRL Laboratories, LLC. Further information is contained in a TSP (see page 1). NPO-30127*

Piezoelectric Diffraction-Based Optical Switches

Switching times can be short enough for demanding applications.

Ames Research Center, Moffett Field, California

Piezoelectric diffraction-based optoelectronic devices have been invented to satisfy requirements for switching signals quickly among alternative optical paths in optical communication networks. These devices are capable of operating with switching times as short as microseconds or even nanoseconds in some cases.

The basic principle of this invention can be illustrated with reference to a simple optical switch shown schematically in the figure. Light of wavelength λ is introduced via an input optical fiber. After emerging from the tip of the input optical fiber, the light passes through a uniform planar diffraction grating that is either made of a piezoelectric material or is made of a non-piezoelectric material bonded tightly to a piezoelectric substrate. A voltage can be applied to
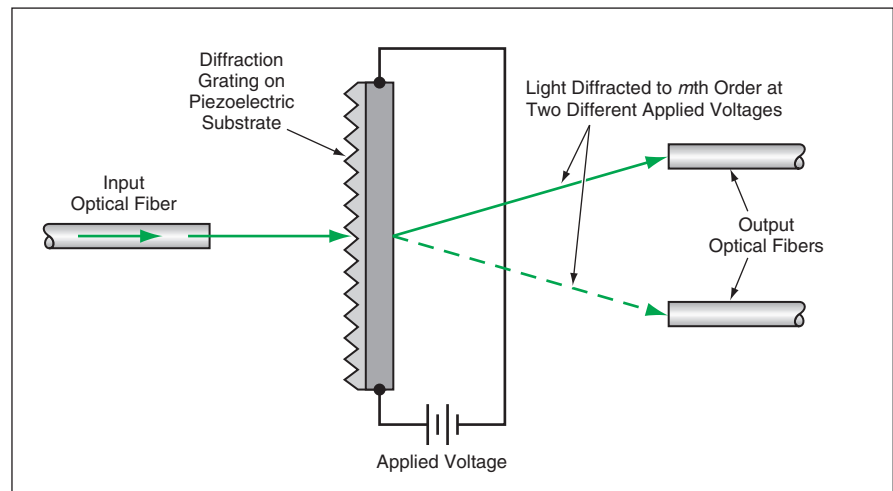
The **Period of the Diffraction Grating Is Varied** between two values by switching between two values of voltage applied to the piezoelectric substrate, thereby switching between two different angles of *m*th-order diffraction. Output optical fibers are positioned to intercept the diffracted light at the two angles.

the piezoelectric member via electrodes at its ends to vary the spatial period of the grating. Two output optical fibers are positioned near the grating, opposite the input fiber.

The angle of diffraction of λ-wavelength light to any given order, m, depends upon the wavelength, the angle of incidence, and the spatial period of the grating. Hence, for a given fixed angle of incidence, one can change the angle of mth-order diffraction by varying applied voltage. The relative positions and orientations of the input fiber, the grating, and the output optical fibers are chosen in conjunction with the grating period so that (1) when no voltage or a given fixed voltage is applied, the mth-order-diffracted light of wavelength λ impinges on one of the output optical fibers and (2) when a different given fixed voltage is applied, the mth-order-diffracted light of wavelength λ impinges on the other out-put optical fiber. Thus, by switching the applied voltage between the two given fixed values, one switches the light between the two output optical paths.

It is also possible to make the device described above perform the following additional functions:

• If only one output optical fiber is used to intercept mth-order-diffracted light and the input light includes multiple wavelengths, then the output wavelength can be selected by applying a corresponding voltage to the piezoelectric member.

• For given fixed values of the angle of incidence, diffraction angle, and wavelength, one can choose a discrete value of applied voltage to select a given diffraction order.

• For given fixed values of the diffraction angle and wavelength, it is possible to vary the applied voltage to switch among different angles of incidence in order to select among different inputs.

Of course, it is possible to design devices more complex than that illustrated in the figure. For example, a device could contain crossed piezoelectric gratings for switching between an input optical fiber and multiple output optical fibers terminated in a planar array. Other examples could include devices that produce more complex switching effects by means of curved gratings, chirped gratings, and/or multiple piezoelectric actuators that bend or twist grating surfaces or that vary grating spatial periods along multiple coordinate axes.

Software

Numerical Modeling of Nanoelectronic Devices

Nanoelectronic Modeling 3-D (NEMO 3-D) is a computer program for numerical modeling of the electronic structure properties of a semiconductor device that is embodied in a crystal containing as many as 16 million atoms in an arbitrary configuration and that has overall dimensions of the order of tens of nanometers. The underlying mathematical model represents the quantum-mechanical behavior of the device resolved to the atomistic level of granularity. The system of electrons in the device is represented by a sparse Hamiltonian matrix that contains hundreds of millions of terms. NEMO 3-D solves the matrix equation on a Beowulf-class cluster computer, by use of a parallel-processing matrix·vector multiplication algorithm coupled to a Lanczos and/or Rayleigh-Ritz algorithm that solves for eigenvalues. In a recent update of NEMO 3-D, a new strain treatment, parameterized for bulk material properties of GaAs and InAs, was developed for two tight-binding submodels. The utility of the NEMO 3-D was demonstrated in an atomistic analysis of the effects of disorder in alloys and, in particular, in bulk $In_xGa_{1-x}As$ and in $In_{0.6}Ga_{0.4}As$ quantum dots.

This program was written by Gerhard Klimeck, Fabiano Oyafuso, R. Chris Bowen, and Timothy Boykin of Caltech for **NASA's Jet Propulsion Laboratory**. *Further information is contained in a TSP (see page 1).*

This software is available for commercial licensing. Please contact Don Hart of the California Institute of Technology at (818) 393-3425. Refer to NPO-30520.

Organizing Diverse, Distributed Project Information

SemanticOrganizer is a software application designed to organize and integrate information generated within a distributed organization or as part of a project that involves multiple, geographically dispersed collaborators. SemanticOrganizer incorporates the capabilities of database storage, document sharing, hypermedia navigation, and semantic-interlinking into a system that can be customized to satisfy the specific information-management needs of different user communities. The program provides a centralized repository of information that is both secure and accessible to project collaborators via the World Wide Web. SemanticOrganizer's repository can be used to collect diverse information (including forms, documents, notes, data, spreadsheets, images, and sounds) from computers at collaborators' work sites. The program organizes the information using a unique network-structured conceptual framework, wherein each node represents a data record that contains not only the original information but also metadata (in effect, standardized data that characterize the information). Links among nodes express semantic relationships among the data records. The program features a Web interface through which users enter, interlink, and/or search for information in the repository. By use of this repository, the collaborators have immediate access to the most recent project information, as well as to archived information. A key advantage to SemanticOrganizer is its ability to interlink information together in a natural fashion using customized terminology and concepts that are familiar to a user community.

Software development activities were directed by Richard M. Keller of **Ames Research Center**. *For further information, access http://sciencedesk.arc.nasa.gov and http://io.arc.nasa.gov.*

Inquiries concerning rights for the commercial use of this invention should be addressed to the Patent Counsel, Ames Research Center, (650) 604-5104. Refer to ARC-15070-1.

Eigensolver for a Sparse, Large Hermitian Matrix

A parallel-processing computer program finds a few eigenvalues in a sparse Hermitian matrix that contains as many as 100 million diagonal elements. This program finds the eigenvalues faster, using less memory, than do other, comparable eigensolver programs. This program implements a Lanczos algorithm in the American National Standards Institute/International Organization for Standardization (ANSI/ISO) C computing language, using the Message Passing Interface (MPI) standard to complement an eigensolver in PARPACK. [PARPACK (Parallel Arnoldi Package) is an extension, to parallel-processing computer architectures, of ARPACK (Arnoldi Package), which is a collection of Fortran 77 subroutines that solve large-scale eigenvalue problems.] The eigensolver runs on Beowulf clusters of computers at the Jet Propulsion Laboratory (JPL). The package is open-source software and is distributed under the terms of the GNU Lesser General Public License (LGPL) on the Internet through the Open Channel Foundation at http://www.openchannelsoftware.com/.

This program was written by E. Robert Tisdale, Fabiano Oyafuso, Gerhard Klimeck, and R. Chris Brown of Caltech for **NASA's Jet Propulsion Laboratory**. *Further information is contained in a TSP (see page 1).*

This software is available for commercial licensing. Please contact Don Hart of the California Institute of Technology at (818) 393-3425. Refer to NPO-30834.

Modified Polar-Format Software for Processing SAR Data

HMPF is a computer program that implements a modified polar-format algorithm for processing data from spaceborne synthetic-aperture radar (SAR) systems. Unlike prior polar-format processing algorithms, this algorithm is based on the assumption that the radar signal wavefronts are spherical rather than planar. The algorithm provides for resampling of SAR pulse data from slant range to radial distance from the center of a reference sphere that is nominally the local Earth surface. Then, invoking the projection-slice theorem, the resampled pulse data are Fourier-transformed over radial distance, arranged in the wavenumber domain according to the acquisition geometry, resampled to a Cartesian grid, and inverse-Fourier-transformed. The result of this process is the focused SAR image. HMPF, and perhaps other programs that implement variants of the algorithm, may give better accuracy than do prior algorithms for processing strip-map SAR data from high altitudes and may give better phase preservation relative to prior polar-format algorithms for processing spotlight-mode SAR data.

This program was written by Curtis Chen of Caltech for **NASA's Jet Propulsion Laboratory**. *Further information is contained in a TSP (see page 1). This software is available for commercial licensing. Please contact Don Hart of the California Institute of Technology at (818) 393-3425. Refer to NPO-30906.*

⚙ e-Stars Template Builder

e-Stars Template Builder is a computer program that implements a concept of enabling users to rapidly gain access to information on projects of NASA's Jet Propulsion Laboratory. The information about a given project is not stored in a data base, but rather, in a network that follows the project as it develops. e-Stars Template Builder resides on a server computer, using Practical Extraction and Reporting Language (PERL) scripts to create what are called "e-STARS node templates," which are software constructs that allow for project-specific configurations. The software resides on the server and does not require specific software on the user machine except for an Internet browser. A user's computer need not be equipped with special software (other than an Internet-browser program). e-Stars Template Builder is compatible with Windows, Mac-intosh, and UNIX operating systems. A user invokes e-Stars Template Builder from a browser window. Operations that can be performed by the user include the creation of child processes and the addition of links and descriptions of documentation to existing pages or nodes. By means of this addition of "child processes" of nodes, a network that reflects the development of a project is generated.

This program was written by Brian Cox of Caltech for **NASA's Jet Propulsion Laboratory**. *Further information is contained in a TSP (see page 1).*

This software is available for commercial licensing. Please contact Don Hart of the California Institute of Technology at (818) 393-3425. Refer to NPO-40089.

⚛ Software for Acoustic Rendering

SLAB is a software system that can be run on a personal computer to simulate an acoustic environment in real time. SLAB was developed to enable computational experimentation in which one can exert low-level control over a variety of signal-processing parameters, related to spatialization, for conducting psychoacoustic studies. Among the parameters that can be manipulated are the number and po-sition of reflections, the fidelity (that is, the number of taps in finite-impulse-response filters), the system latency, and the update rate of the filters. Another goal in the development of SLAB was to provide an inexpensive means of dynamic synthesis of virtual audio over headphones, without need for special-purpose signal-processing hardware. SLAB has a modular, object-oriented design that affords the flexibility and extensibility needed to accommodate a variety of computational experiments and signal-flow structures. SLAB's spatial renderer has a fixed signal-flow architecture corresponding to a set of parallel signal paths from each source to a listener. This fixed architecture can be regarded as a compromise that optimizes efficiency at the expense of complete flexibility. Such a compromise is necessary, given the design goal of enabling computational psychoacoustic experimentation on inexpensive personal computers.

This program was written by Joel D. Miller of QSS Group, Inc., for **Ames Research Center**. *For further information, access http://human-factors.arc.nasa.gov/SLAB/. Refer to ARC-14991-1.*

Functionally Graded Nanophase Beryllium/Carbon Composites

The main advantage, relative to Co/WC/diamond composites, is less weight.

Lyndon B. Johnson Space Center, Houston, Texas

Beryllium, beryllium alloys, beryllium carbide, and carbon are the ingredients of a class of nanophase $Be/Be_2C/C$ composite materials that can be formulated and functionally graded to suit a variety of applications. In a typical case, such a composite consists of a first layer of either pure beryllium or a beryllium alloy, a second layer of B_2C, and a third layer of nanophase sintered carbon derived from fullerenes and nanotubes. The three layers are interconnected through interpenetrating spongelike structures.

These $Be/Be_2C/C$ composite materials are similar to Co/WC/diamond functionally graded composite materials, except that (1) W and Co are replaced by Be and alloys thereof and (2) diamond is replaced by sintered carbon derived from fullerenes and nanotubes. (Option-

ally, one could form a $Be/Be_2C/dia$-mond composite.) Because Be is lighter than W and Co, the present $Be/Be_2C/C$ composites weigh less than do the corresponding Co/WC/diamond composites. The nanophase carbon is almost as hard as diamond.

WC/Co is the toughest material. It is widely used for drilling, digging, and machining. However, the fact that W is a heavy element (that is, has high atomic mass and mass density) makes W unattractive for applications in which weight is a severe disadvantage. Be is the lightest tough element, but its toughness is less than that of WC/Co alloy. Be strengthened by nanophase carbon is much tougher than pure or alloy Be. The nanophase carbon has an unsurpassed strength-to-weight ratio.

The $Be/Be_2C/C$ composite materials are especially attractive for terrestrial and aerospace applications in which there are requirements for light weight along with the high strength and toughness of the denser Co/WC/diamond materials. These materials could be incorporated into diverse components, including cutting tools, bearings, rocket nozzles, and shields. Moreover, because Be and C are effective as neutron moderators, $Be/Be_2C/C$ composites could be attractive for some nuclear applications.

This work was done by Oleg A. Voronov and Gary S. Tompa of Diamond Materials Inc. for **Johnson Space Center**. *Further information is contained in a TSP (see page 1)..* MSC-23274

Thin Thermal-Insulation Blankets for Very High Temperatures

One blanket would have about the thickness of several sheets of paper.
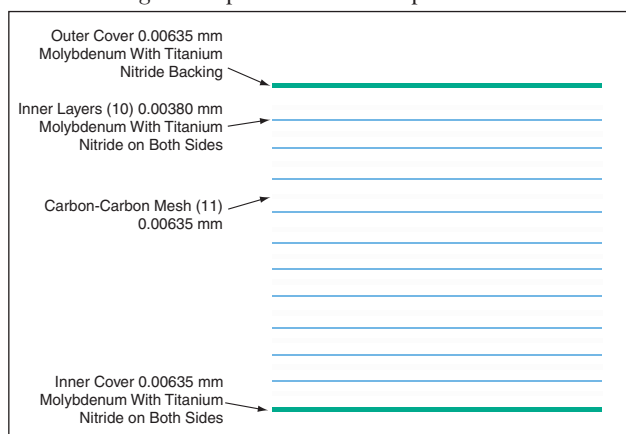
Goddard Space Flight Center, Greenbelt, Maryland

Thermal-insulation blankets of a proposed type would be exceptionally thin and would endure temperatures up to 2,100 °C. These blankets were originally intended to protect components of the NASA Solar Probe spacecraft against radiant heating at its planned closest ap-

proach to the Sun (a distance of 4 solar radii). These blankets could also be used on Earth to provide thermal protection in special applications (especially in vacuum chambers) for which conventional thermal-insulation blankets would be too thick or would not perform adequately.

A blanket according to the proposal (see figure) would be made of molybdenum, titanium nitride, and carbon-carbon composite mesh, which melt at temperatures of 2,610, 2,930, and 2,130 °C, respectively. The emittance of molybdenum is 0.24, while that of titanium nitride is 0.03. Carbon-carbon composite mesh is a thermal insulator.

Typically, the blanket would include

0.25-mil (≈0.00635-mm)-thick hot-side and cold-side cover layers of molybdenum. Titanium nitride would be vapor-deposited on both surfaces of each cover layer. Between the cover layers there would be 10 inner layers of 0.15-mil (≈0.0038-mm)-thick molybdenum with vapor-deposited titanium nitride on both sides of each layer. The thickness of each titanium nitride coat would be about 1,000 Å. The cover and inner layers would be interspersed with 0.25-mil (0.00635-mm)-thick layers of carbon-carbon composite mesh. The blanket would have total thickness of 4.75 mils (≈0.121 mm) and an areal mass density of 0.7 kg/m^2. One could, of course, increase the thermal-insulation capability of the blanket by increasing number of inner layers (thereby unavoidably increasing the total thickness and mass density).

This work was done by Michael K. Choi of **Goddard Space Flight Center.** *Further information is contained in a TSP (see page 1). GSC-14386*

Outer Cover 0.00635 mm Molybdenum With Titanium Nitride Backing

Inner Layers (10) 0.00380 mm Molybdenum With Titanium Nitride on Both Sides

Carbon-Carbon Mesh (11) 0.00635 mm

Inner Cover 0.00635 mm Molybdenum With Titanium Nitride on Both Sides

This **Thermal-Insulation Blanket** would be very thin and lightweight. The blanket would be made of materials that melt at temperatures greater than 2,100 °C.

Prolonging Microgravity on Parabolic Airplane Flights

Techniques for improving the approximation of free fall are proposed.

Goddard Space Flight Center, Greenbelt, Maryland

Three techniques have been proposed to prolong the intervals of time available for microgravity experiments aboard airplanes flown along parabolic trajectories. Typically, a pilot strives to keep an airplane on such a trajectory during a nominal time interval as long as 25 seconds, and an experimental apparatus is released to float freely in the airplane cabin to take advantage of the microgravitational environment of the trajectory for as long as possible. It is usually not possible to maintain effective microgravity during the entire nominal time interval because random aerodynamic forces and fluctuations in pilot control inputs cause the airplane to deviate slightly from a perfect parabolic trajectory (see figure), such that the freely floating apparatus bumps into the ceiling, floor, or a wall of the airplane before the completion of the parabola. Heretofore, free-float times have tended to be no longer than a few seconds.

One of the proposed techniques is to release the experimental apparatus at some point along the trajectory chosen to maximize the free-float time. A statistical analysis of flight acceleration data has revealed that the best release time is the third instant, during the nominal parabola interval, when the acceleration along the z axis crosses zero. (The z axis is defined here as the floor-to-ceiling axis in a coordinate system attached to the airplane.) The analysis shows that, assuming a range of motion of 2 m along the z axis, the experimental apparatus could float freely for 8 seconds on about half of all attempts. The analysis also shows that if one is willing to ac-
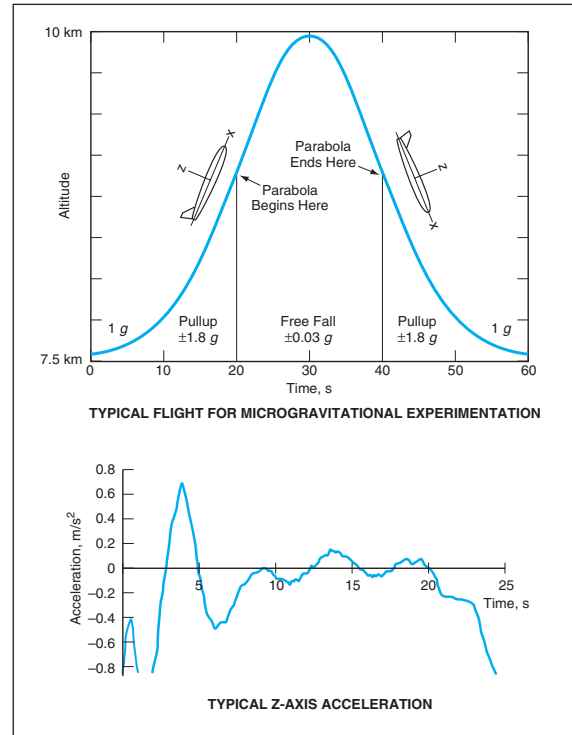
cept acceleration as large as ±0.1 m/s^2 prior to release, then the time available for experimentation could be as long as 10 seconds on about one-third to one-half of all attempts.

The second proposed technique would involve mounting the experimental apparatus on a z-axis rail and damping the motion of the apparatus once it has been released. Simple damping would necessarily entail residual accelerations intermediate between those of rigid mounting and pure free floating. A statistical analysis of flight acceleration data has shown that simple damping with a damping coefficient of 1/2 could prolong experiment times by about one-fourth on average, provided that one could tolerate residual accelerations about half as large as those of the airplane.

The third proposed technique would be an advanced version of the second one. Instead of a simple damper, the mounting system would include (1) one or more sensor(s) for measuring position, velocity, and acceleration of the experimental apparatus along the z axis and (2) an active control system that would strive to keep the acceleration within a desired small range centered at zero while always seeking to return the apparatus to the midpoint of its range of motion. This technique

TYPICAL FLIGHT FOR MICROGRAVITATIONAL EXPERIMENTATION

TYPICAL Z-AXIS ACCELERATION

Residual Acceleration is experienced by an object fixed to an airplane that is nominally flying along a parabolic trajectory to approximate a free fall.

would make it possible to maintain acceleration within ±0.005 *g* [where *g* = normal Earth gravitational acceleration (about 9.8 m/s^2)] for at least 10 seconds on half of all attempts, or to maintain an acceleration within ±0.01 *g* for 10 seconds on about two-thirds of all attempts.

This work was done by David W. Robinson of **Goddard Space Flight Center**. *Further information is contained in a TSP (see page 1). GSC-14521*

Device for Locking a Control Knob

John F. Kennedy Space Center, Florida

A simple, effective, easy-to-use device locks a control knob in a set position. In the initial application for which this device was conceived, the control knob to be locked is that of a needle valve. Pre-

viously, in that application, it was necessary for one technician to hold the knob to keep the valve at the desired flow setting while another technician secured the valve with safety wire — a time-con-

suming procedure. After attachment of the wire, it was still possible to turn the knob somewhat. In contrast, a single technician using the present device can secure the knob in the desired position

in about 30 seconds, and the knob cannot thereafter be turned, even in the presence of harsh vibrations, which occur during space shuttle launch. The device includes a special-purpose clamp that fits around the control knob and its shaft and that can be tightened onto the knob, without turning the knob, by means of two thumbscrews. The end of the device opposite the clamp is a tang that contains a slot that, in turn, engages a bolt that protrudes from the panel on which the control knob and its shaft are mounted.

☢ Cable-Dispensing Cart

John F. Kennedy Space Center, Florida

A versatile cable-dispensing cart can support as many as a few dozen reels of cable, wire, and/or rope. The cart can be adjusted to accommodate reels of various diameters and widths, and can be expanded, contracted, or otherwise reconfigured by use of easily installable and removable parts that can be carried onboard. Among these parts are dispensing rods and a cable guide that enables dispensing of cables without affecting the direction of pull. Individual reels can be mounted on or removed from the cart without affecting the other reels: this feature facilitates the replacement or reuse of partially depleted reels, thereby helping to reduce waste. Multiple cables, wires, or ropes can be dispensed simultaneously. For maneuverability, the cart is mounted on three wheels. Once it has been positioned, the cart is supported by rubber mounts for stability and for prevention of sliding or rolling during dispensing operations. The stability and safety of the cart are enhanced by a low-center-of-gravity design. The cart can readily be disassembled into smaller units for storage or shipping, then reassembled in the desired configuration at a job site.

Foam Sensor Structures Would Be Self-Deployable and Survive Hard Landings

NASA's Jet Propulsion Laboratory, Pasadena, California

A document proposes systems of sensors encased in cold hibernated elastic memory (CHEM) structures for exploring remote planets. The CHEM concept was described in two prior *NASA Tech Briefs* articles, including "Cold Hibernated Elastic Memory (CHEM) Expandable Structures" (NPO-20394), Vol. 23, No. 2 (February 1999), page 56 and "Solar Heating for Deployment of Foam Structures" (NPO-20961), Vol. 25, No. 10 (October 2001), page 36. To recapitulate: Lightweight structures that can be compressed for storage and later expanded, then rigidified for use are made from foams of shape-memory polymers (SMPs). According to the instant proposal, a CHEM sensor structure would be fabricated at full size from SMP foam at a temperature below its glass-transition temperature (T_g). It would then be heated above T_g and compacted to a small volume, then cooled below T_g and kept below T_g during launch, flight, and landing. At landing, the inelastic yielding of the rigid compacted foam would absorb impact energy, thereby enabling the structure to survive the landing. The structure would then be solar heated above T_g, causing it to revert to its original size and shape. Finally, the structure would be rigidified by cooling it below T_g by the cold planetary or space environment. Besides surviving hard landing, this sensor system will provide a soft, stick-at-the-impact-site landing to access scientifically and commercially interesting sites, including difficult and hard-to-reach areas.

This work was done by Witold Sokolowski and Eric Baumgartner of Caltech for **NASA's Jet Propulsion Laboratory**. *Further information is contained in a TSP (see page 1).*
NPO-30654

Real-Gas Effects on Binary Mixing Layers

NASA's Jet Propulsion Laboratory, Pasadena, California

This paper presents a computational study of real-gas effects on the mean flow and temporal stability of heptane/nitrogen and oxygen/hydrogen mixing layers at supercritical pressures. These layers consist of two counterflowing free streams of different composition, temperature, and density. As in related prior studies reported in *NASA Tech Briefs*, the governing conservation equations were the Navier-Stokes equations of compressible flow plus equations for the conservation of total energy and of chemical-species masses. In these equations, the expressions for heat fluxes and chemical-species mass fluxes were derived from fluctuation-dissipation theory and incorporate Soret and Dufour effects. Similarity equations for the streamwise velocity, temperature, and mass fractions were derived as approximations to the governing equations. Similarity profiles showed important real-gas, non-ideal-mixture effects, particularly for temperature, in departing from the error-function profile, which is the similarity solution for incompressible flow. The temperature behavior was attributed to real-gas thermodynamics and variations in Schmidt and Prandtl numbers. Temporal linear inviscid stability analyses were performed using the similarity and error-function profiles as the mean flow. For the similarity profiles, the growth rates were found to be larger and the wavelengths of highest instability shorter, relative to those of the error-function profiles and to those obtained from incompressible-flow stability analysis. The range of unstable wavelengths was found to be larger for the similarity profiles than for the error-function profiles.

This work was done by Nora Okong'o and Josette Bellan of Caltech for **NASA's Jet Propulsion Laboratory**. *Further information is contained in a TSP (see page 1).*
NPO-40162

Earth-Space Link Attenuation Estimation via Ground Radar Kdp

Lyndon B. Johnson Space Center, Houston, Texas

A method of predicting attenuation on microwave Earth/spacecraft communication links, over wide areas and under various atmospheric conditions, has been developed. In the area around the ground station locations, a nearly horizontally aimed polarimetric S-band ground radar measures the specific differential phase (Kdp) along the Earth-space path. The specific attenuation along a path of interest is then computed by use of a theoretical model of the relationship between the measured S-band specific differential phase and the specific attenuation at the frequency to be used on the communication link. The model includes effects of rain, wet ice, and other forms of precipitation.

The attenuation on the path of interest is then computed by integrating the specific attenuation over the length of the path. This method can be used to determine statistics of signal degradation on Earth/spacecraft communication links. It can also be used to obtain real-time estimates of attenuation along multiple Earth/spacecraft links that are parts of a communication network operating within the radar coverage area, thereby enabling better management of the network through appropriate dynamic routing along the best combination of links.

Wedge Heat-Flux Indicators for Flash Thermography

Lyndon B. Johnson Space Center, Houston, Texas

Wedge indicators have been proposed for measuring thermal radiation that impinges on specimens illuminated by flash lamps for thermographic inspection. Heat fluxes measured by use of these indicators would be used, along with known thermal, radiative, and geometric properties of the specimens, to estimate peak flash temperatures on the specimen surfaces. These indicators would be inexpensive alternatives to high-speed infrared pyrometers, which would otherwise be needed for measuring peak flash surface temperatures. The wedge is made from any suitable homogenous material such as plastic. The choice of material is governed by the equation given below. One side of the wedge is covered by a temperature sensitive compound that decomposes irreversibly when its temperature exceeds a rated temperature (T_{rated}). The uncoated side would be positioned alongside or in place of the specimen and exposed to the flash, then the wedge thickness (d) at the boundary between the white and blackened portions measured. The heat flux (Q) would then be estimated by

$$Q = (c\rho/\varepsilon_b)(T_{rated} - T_{ambient})d,$$

where c and ρ are the specific heat and mass density, respectively, of the wedge material; ε_b is the emissivity of the black layer of the sheet material, and $T_{ambient}$ is the ambient temperature.

Measuring Diffusion of Liquids by Common-Path Interferometry
Diffusivities are computed from time series of interferograms.

John H. Glenn Research Center, Cleveland, Ohio

A method of observing the interdiffusion of a pair of miscible liquids is based on the use of a common-path interferometer (CPI) to measure the spatially varying gradient of the index refraction in the interfacial region in which the interdiffusion takes place. Assuming that the indices of refraction of the two liquids are different and that the gradient of the index of refraction of the liquid is proportional to the gradient in the relative concentrations of either liquid, the diffusivity of the pair of liquids can be calculated from the temporal variation of the spatial variation of the index of refraction. This method yields robust measurements and does not require precise knowledge of the indices of refraction of the pure liquids. Moreover, the CPI instrumentation is compact and is optomechanically robust by virtue of its common-path design.

The two liquids are placed in a transparent rectangular parallelepiped test cell. Initially, the interface between the liquids is a horizontal plane, above which lies pure liquid 2 (the less-dense liquid) and below which lies pure liquid 1 (the denser liquid). The subsequent interdiffusion of the liquids gives rise to a gradient of concentration and a corresponding gradient of the index of refraction in a mixing layer. For the purpose of observing the interdiffusion, the test cell is placed in the test section of the CPI, in which a collimated, polarized beam of light from a low-power laser is projected horizontally through a region that contains the mixing layer.

The CPI used in this method is a shearing interferometer. Like other shearing interferometers, this CPI can also be characterized as a schlieren interferometer because its optical setup is partly similar to that of schlieren system. However, the basic principle of operation of this CPI applies to the case in which refraction is relatively weak so that unlike in a schlieren system, rays of light propagating through the test cell can be assumed not to be bent, but, rather, delayed (and correspondingly changed in phase) by amounts proportional to the indices of refraction along their paths. After passing through the test cell, the beam is focused on a Wollaston prism, which splits the beam into two beams that are slightly displaced from each other. When the beams are recombined, they produce interference fringes that indicate gradients of refraction in the test cell. A charge-coupled-device (CCD) camera captures the interferograms, and a video recorder stores them for later analysis.

The interferometer optics are arranged for operation in a mode, known in the art as the finite-fringe mode, in which equidistant, parallel interference fringes appear when the index of refraction in the test cell is uniform (as is the case when only one fluid is present). When a second liquid is introduced and diffusion occurs, the deviation or shift of a fringe from its undisturbed location is a measure of the gradient of the index of refraction in the test cell. For the purpose of this method, it is assumed that the index of
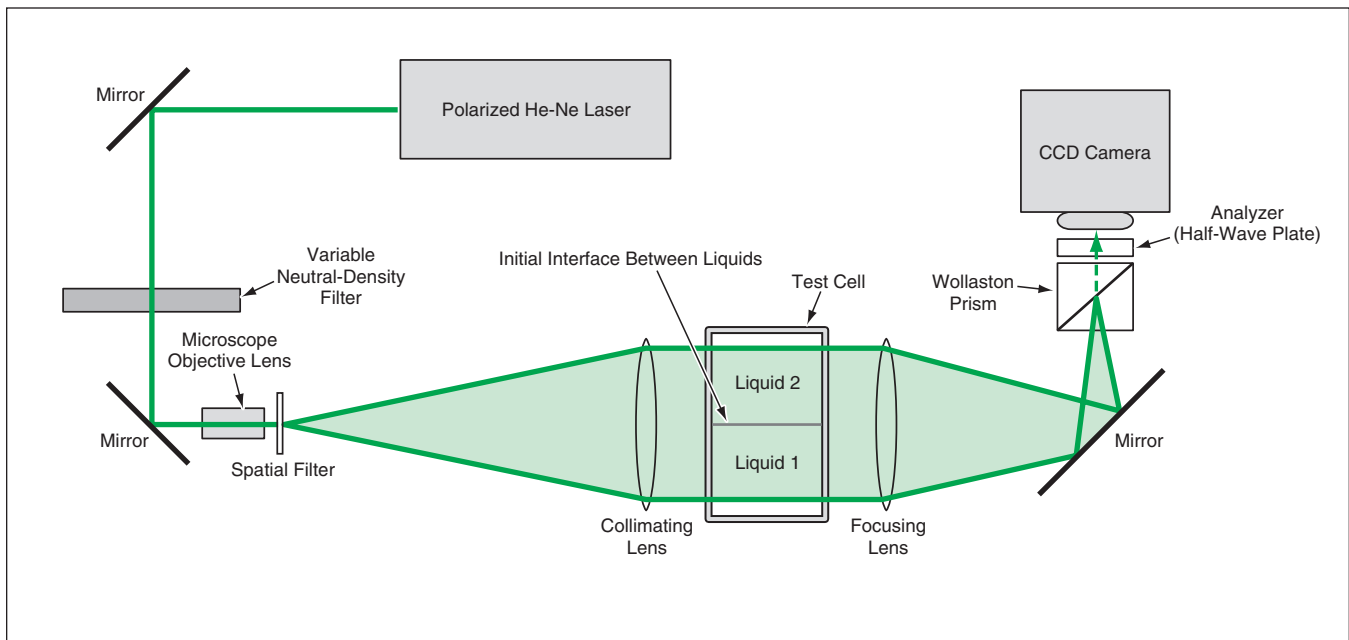
A **Common-Path Interferometer** projects a polarized, collimated horizontal light beam through a test cell that contains two pure liquids and a mixing layer between them.

refraction is horizontally uniform and varies only as a function of height above or below the initial interfacial plane.

An important element of the present method is rotation of the Wollaston prism around its optical axis by a small amount chosen so that the interference fringes form at a slight angle with respect to the initial interface between the liquids. The advantage of this angle is

not intuitively obvious, and can be understood only in terms of the applicable equations. In summary, what the equations show is that proper choice of the angle results in magnification of the visual effect of the gradient of concentration in the mixing zone. Without the proper choice of the angle, the interference-fringe image cannot be interpreted simply or used to obtain the diffusivity of the fluids.

Zero-Shear, Low-Disturbance Optical Delay Line

The only optical components would be two flat mirrors.

NASA's Jet Propulsion Laboratory, Pasadena, California

A design concept has been proposed for an optomechanical apparatus that would implement a variable optical delay line with a fixed angle between its input and output light beams. The apparatus would satisfy requirements that emphasize performance in interferometric applications: to contain a minimum number of optical surfaces, each used at low angle-of-incidence, and to be nominally free of shear (transverse motion of the beam) on any optical element. As an additional advantage, the apparatus would afford partial compensation of vibration disturbances associated with adjustment of the optical delay by both reducing the amount of motion required to achieve a desired optical delay and by splitting the total

motion between two assemblies. As compared to prior art implementations of delay lines, the only disadvantage of the concept is that the motions of the optical elements must be well coordinated through mechanical linkages or electronic controls.

The figure depicts a typical configuration of the apparatus. The optical elements would be two flat mirrors — M1 and M2 — mounted on linear actuators. The actuation axes of M1 and M2 would be parallel to the incoming and outgoing light beams, respectively. M1 would be mounted on its actuator at a fixed angle required to aim the beam reflected from it to the center of M2. In turn, M2 would be mounted on its actuator at a fixed angle required to aim

the outgoing beam in the desired direction. Moreover, the angles of M1 and M2 would be chosen so that the angle between M1 and the incoming beam equals the angle between M2 and the outgoing beam.

All of the properties of this apparatus that make it preferable to prior variable optical delay lines depend on making M1 and M2 move by equal and opposite amounts to vary the length of the optical path: In shortening (or lengthening) the optical path, one must move M1 a required distance along the input beam path toward (or away from) M2 while moving M2 along the same distance along the output-beam path toward (or away from) M1. It is noted that the path length change introduced by the linear

motion of each mirror is greater than just the distance actually traversed by the mirror. In most configurations, the path length change effected by the delay line is more than 3 times the actual distance moved by either mirror.

As a result of this geometric arrangement and coordination of motions, the incoming beam would always strike M1 at the same point, the beam reflected from M1 would always strike M2 at the same point, and the outgoing beam would always strike the next optical element in the output path at the same point, giving zero beam shear at all times. Assuming that the mirrors and their associated mounts would have equal masses, the vector component of the motions of the mirrors along the line joining the centers of the mirrors would introduce no net momentum disturbance, and thereby no significant vibrational perturbations into the surrounding structure. There would remain a small, uncompensated vector component of momentum disturbance along the direction perpendicular to the line between the centers of the mirrors; optionally, one could compensate for this component of momentum disturbance by use of a relatively small auxiliary moving mass.

This work was done by Jeffrey Oseas of Caltech for **NASA's Jet Propulsion Laboratory**. *Further information is contained in a TSP (see page 1).*
NPO-30820
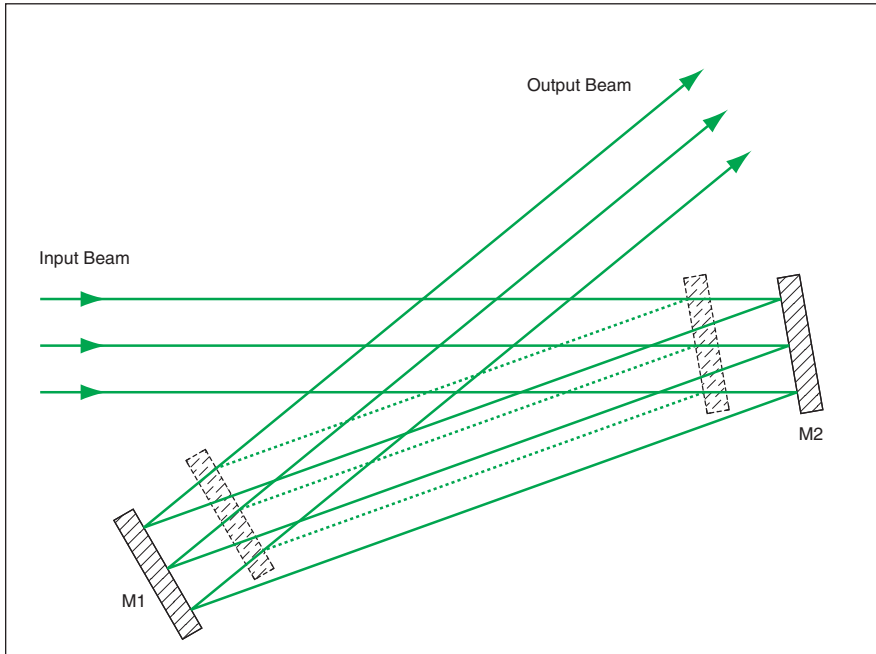
Coordinated Motion of Mirror M1 and Mirror M2 along the input and output axis, respectively, would ensure that the light beam remained centered on both M1 and M2 at all times.
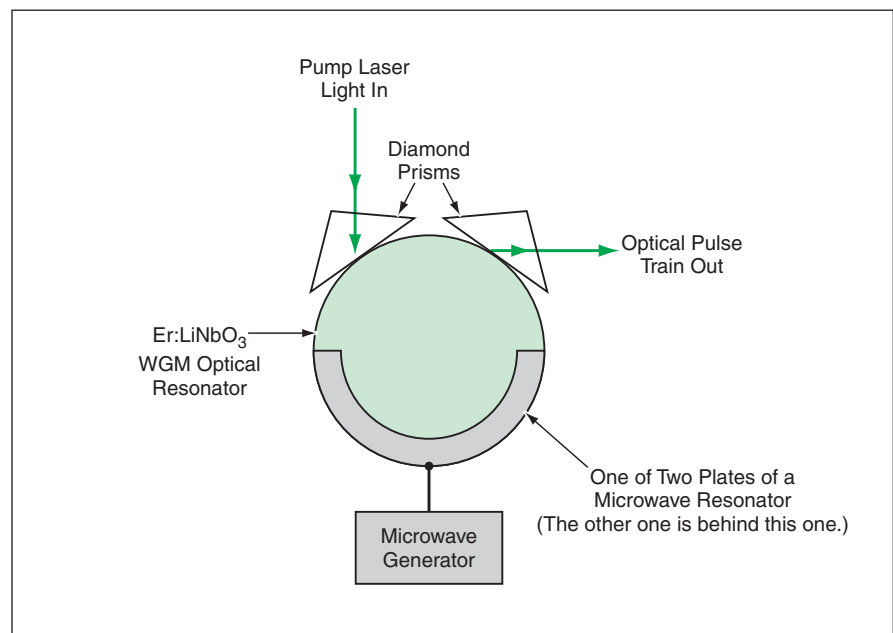
Whispering-Gallery Mode-Locked Lasers

Compact devices would generate optical pulses at repetition rates of tens of gigahertz.

NASA's Jet Propulsion Laboratory, Pasadena, California

Mode-locked lasers of a proposed type would incorporate features of the design and operation of previously demonstrated miniature electro-optical modulators and erbium-doped glass lasers that contain whispering-gallery-mode (WGM) resonators. That is to say, WGM lasers and WGM electro-optical modulators would be integrated into monolithic units that, when suitably excited with pump light and microwaves, would function as mode-locked lasers. The proposed devices are intended to satisfy an anticipated demand for compact, low-power devices that could operate in the optical-communication wavelength band centered at a wavelength of 1.55 µm and could generate pulses as short as picoseconds at repetition rates of multiple gigahertz.

A representative device according to the proposal (see figure) would include a WGM optical resonator in the form of an oblate spheroid or disk that would have a diameter of the order of a millimeter and would be made from z-cut lithium nio-

A **Whispering-Gallery Mode-Locked Laser** would include a WGM optical resonator made of an optically nonlinear material placed between plates of a microwave resonator so that the microwave and optical resonators would also function as an electro-optical modulator that would couple the microwave and optical fields.

bate doped with erbium (Er:LiNbO₃). The oblateness of the spheroid or disk would be essential for suppressing undesired electromagnetic modes of the resonator. Continuous-wave (CW) pump laser light at a wavelength of 1.48 μm would be coupled into the WGM optical resonator via a diamond prism. Light would be coupled out of the optical resonator via another diamond prism. As a result of the interaction between the pump light and the dopant erbium ions, modes at wavelengths in the vicinity of 1.54 μm would be amplified. In the absence of the design features described below, the device as described thus far would emit CW light in the 1.54-μm wavelength band.

The optical resonator would be placed between two plates of a microwave resonator. By adjusting the shape of the microwave resonator, one could adjust the frequency of resonance of the microwave field to fit the difference between the frequencies of successive modes of the optical resonator. Under this condition, the nonlinearity of dielectric response of LiNbO₃ would serve to couple the modes of the microwave and optical resonators.

Because of the optical/microwave coupling, the device would function as a mode-locked laser in the presence of both CW pump light and CW microwave radiation. The net result of the interaction would be the generation of pulses of light in the WGM optical resonator. Because the optical amplification would not be sensitive to phase, pulses are expected to travel circumferentially around the resonator in both directions. Hence, for example, it should be possible to extract an optical pulse train propagating in the circumferential direction opposite of that of the pump light, as shown in the figure.

The performance of the device has been estimated theoretically on the basis of the underlying physical principles and the performances of prior WGM electro-optical modulators and erbium-doped glass lasers: Pulse durations as short as several picoseconds and pulse-repetition rates of tens of gigahertz should be readily achievable, and it may be possible to reach repetition rates as high as 100 GHz. The required microwave power is expected to be no more than a few milliwatts. The pump power is expected to range from a threshold value as low as several microwatts to a maximum value high enough to yield the CW equivalent of several milliwatts of output. With respect to pulse-repetition rates and power efficiency, the proposed device would perform better than any prior device designed to satisfy the same requirements.

Spatial Light Modulators as Optical Crossbar Switches
Optimization computations would take account of realistic characteristics of all optical components.

Lyndon B. Johnson Space Center, Houston, Texas

A proposed method of implementing cross connections in an optical communication network is based on the use of a spatial light modulator (SLM) to form controlled diffraction patterns that connect inputs (light sources) and outputs (light sinks). Sources would typically include optical fibers and/or light-emitting diodes; sinks would typically include optical fibers and/or photodetectors. The sources and/or sinks could be distributed in two dimensions; that is, on planes. Alternatively or in addition, sources and/or sinks could be distributed in three dimensions — for example, on curved surfaces or in more complex (including random) three-dimensional patterns.

The proposed method offers the following advantages over prior methods:
- Invariance to polarization of incoming light;
- Minimization of crosstalk;
- A full connectivity matrix (that is, the possibility of connecting or disconnecting between any input and any output terminal) in a given optical crossbar switch;
- Retention of switched information in light-borne form (in contradistinction to absorption of light, intermediate processing in electronic form, and re-emission of light);
- Accommodation of the undesired but unavoidable coupling of phase and amplitude modulation in a realistic spatial light modulator;
- Automated dynamic alignment of the components of a newly assembled optical crossbar switch;
- Switching in a single stage rather than multiple "butterfly" stages;
- Computational tradeoff among desired but at least partly mutually exclusive switch characteristics (for example, among diffraction efficiency, uniformity of connection strengths, and crosstalk);
- Design for operation in the Fresnel (near-field) diffraction regime rather than in the Fourier (far-field approximation) regime;
- Ability to utilize inexpensive lenses and other less-than-ideal fixed optical elements; and
- Direct (in contradistinction to indirect) optimization of switch properties.

The method incorporates a combination of synergistic techniques and concepts developed to solve problems encountered in prior research on crossbar optical switches. The combination of techniques and concepts is so extremely complex that only a highly abbreviated summary of a few salient features, addressing some of the aforementioned advantages, can be given below.

The issue of polarization arises because the performances of many SLMs affect the polarization of output light and are affected by the polarization of input light. Because it is impractical to guarantee the polarization of input light from disparate sources, it would be better to render a crossbar switch insensitive to input polarization. In a crossbar switch according to
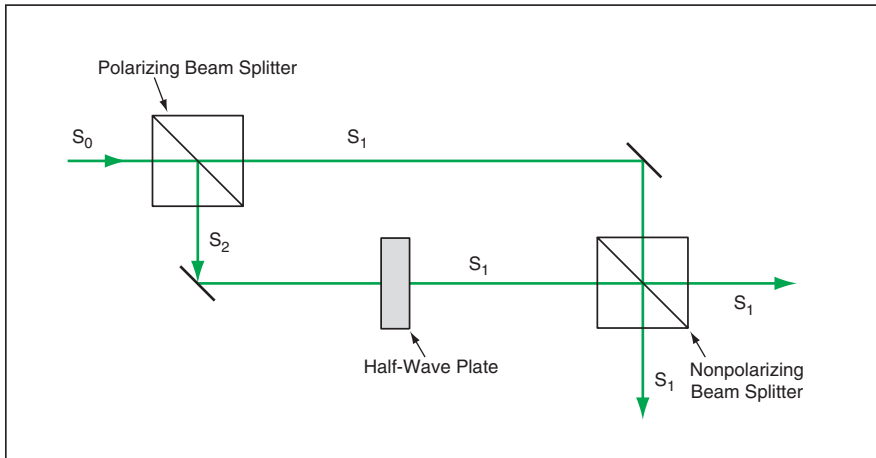
This **Optical Assembly** would convert input light of any polarization (S_0) to two mutually independent polarizations (S_1 and S_2). S_2 would then be further converted to S_1. The output beam would be pure S_1, attenuated from S_0 by a factor of 2.

the proposal, all of the input light would be converted to a single input polarization desired for the SLM by use of an optical assembly like that shown in the figure. The light would be attenuated by a factor of 2 by passage through this assembly, but in a typical case, the disadvantage of this attenuation would be offset by the advantage of obtaining the polarization needed to optimize the performance of the SLM.

The method provides for the choice of input and output locations in a computational optimization process to minimize crosstalk, while making it possible to connect from any desired input terminal(s) to any desired output terminal(s). In this process, the far-field approximation would be irrelevant and unnecessary because one would utilize realistic near-field measured and/or computed diffraction patterns generated by the SLM. The inherently comprehensive nature of the optimization calculations is such that realistic modulation characteristics of the SLM, realistic optical characteristics of all components, alignment or misalignment of components, diffraction efficiency, uniformity or nonuniformity of signal strengths, and crosstalk would all be automatically taken into account.

Update on EMD and Hilbert-Spectra Analysis of Time Series

Goddard Space Flight Center, Greenbelt, Maryland

U.S. Patent 6,381,559 presents further information about the method described in "Analyzing Time Series Using EMD and Hilbert Spectra" (GSC-13817), *NASA Tech Briefs*, Vol. 24, No. 10 (October 2000), page 63. To recapitulate: The method is especially well suited for analyzing time-series data that represent nonstationary and nonlinear physical phenomena. The method is based principally on the concept of empirical mode decomposition (EMD), according to which any complicated signal (as represented by digital samples) can be decomposed into a finite number of functions, called "intrinsic mode functions" (IMFs), that admit well-behaved Hilbert transforms. The local energies and the instantaneous frequencies derived from the IMFs through Hilbert transforms can be used to construct an energy-frequency-time distribution, denoted a Hilbert spectrum. The patent expands on the description in the cited prior article by explaining underlying mathematical principles and describing details of implementation. The patent also describes, as major elements of the method, the options of (1) filtering the original signal by combining a subset of IMFs and (2) fitting a curve to the filtered signal — something that it may not be possible to do with the original signal.

This work was done by Norden E. Huang of **Goddard Space Flight Center**. *Further information is contained in a TSP (see page 1).*

This invention is owned by NASA, and a patent application has been filed. Inquiries concerning nonexclusive or exclusive license for its commercial development should be addressed to the Patent Counsel, Goddard Space Flight Center; (301) 286-7351. Refer to GSC-13817-3.

Quad-Tree Visual-Calculus Analysis of Satellite Coverage
The computational burden is less than in a pixel representation.

NASA's Jet Propulsion Laboratory, Pasadena, California

An improved method of analysis of coverage of areas of the Earth by a constellation of radio-communication or scientific-observation satellites has been developed. This method is intended to supplant an older method in which the global-coverage-analysis problem is solved from a ground-to-satellite perspective. The older method is suitable for coarse-grained analysis of coverage of a constellation of a few satellites, but the algorithms of the older method are too slow and cumbersome for the large scope of the problem of analysis of coverage of a modern constellation of many satellites intended to provide global coverage all the time. In contrast, the present method provides for rapid and efficient analysis. This method is derived from a satellite-to-ground perspective and involves a unique combination of two techniques for multiresolution representation of map features on the surface of a sphere.

The first of the two techniques, called "visual calculus," is one that embodies the satellite-to-ground perspective and assists in the visualization of global coverage. In visual calculus, a satellite can be regarded as "painting" its field of view or other coverage field onto the ground
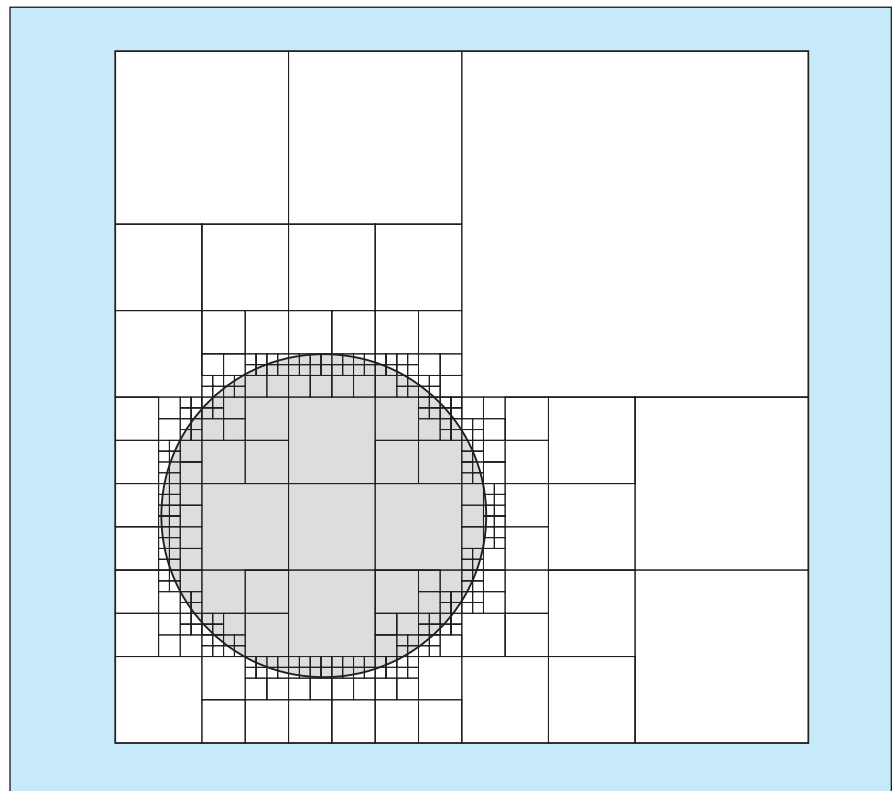
Using a Multiresolution Map to analyze a circular region, it is not necessary to resort to full resolution everywhere. Large areas with the same value can be represented by a few large squares; smaller squares are needed only to resolve details of the boundary.

to generate simple maps. These maps are two-dimensional projections of the globe, with ground tracks and station masks for each satellite in a constellation. These maps are processed further to generate composite maps that answer a variety of simple and complex questions regarding coverage, both for specific ground points and for regions.

For the purpose of computational implementation, a map is represented by an integer function of latitude and longitude, analogous to the more familiar map color as a function of latitude and longitude. More specifically, a map object $\mathbf{M}$ is defined by $\mathbf{M}(l,\lambda):(l,\lambda)\rightarrow i$, where l is latitude, λ is longitude, and i is the integer value at the point in question. The processing of maps to generate composite maps and answer questions about coverage involves, among other things, the use of an algebra in which map objects are manipulated by unary, binary, Boolean, and other operators. Examples of operators include one that finds the distance from a given point to a map boundary and one that

finds what percentage of a map has a given integer value.

The second technique essential to the present method is the use of a quad-tree data structure in implementing the visual calculus. For this purpose, the map function is redefined to provide not only the integer value for a given location but also information on how far one must travel from that location to encounter a change in the map. A point quad tree is well suited to a multiresolution representation of map features on the surface of a sphere.

In essence, a quad tree is a data-compression construct that takes advantage of the facts that (1) a typical map contains only a few regions with a few values and (2) at each point, most values in the neighborhood are the same value. In a quad tree, squares of pixels that have the same value are represented as one large square. It does not become necessary to do calculations on a subdivision of a square until a map boundary subdivides the square. Thus, it is not necessary to fix resolution at the beginning of an analysis. If higher resolution is needed

for a particular map, it can be achieved through finer subdivisions.

The main reason for choosing a quad-tree data structure instead of a pixel-based data structure is that the point-quad-tree structure requires less data-storage space. This computational advantage arises because the number of subdivisions needed in a given case is approximately proportional to the length of the boundary between regions, instead of proportional to the area of the regions as in a pixel representation. It is necessary to subdivide only those squares that straddle a boundary (see figure), and because a boundary is one-dimensional, the number of subdivisions for the required resolution scales linearly, rather than quadratically as when subdividing an area with pixels.

Books & Reports

Dyakonov-Perel Effect on Spin Dephasing in n-Type GaAs

A paper presents a study of the contribution of the Dyakonov-Perel (DP) effect to spin dephasing in electron-donor-doped bulk GaAs in the presence of an applied steady, moderate magnetic field perpendicular to the growth axis of the GaAs crystal. (The DP effect is an electron-wave-vector-dependent spin-state splitting of the conduction band, caused by a spin/orbit interaction in a crystal without an inversion center.) The applicable Bloch equations of kinetics were constructed to include terms accounting for longitudinal optical and acoustic phonon scattering as well as impurity scattering. The contributions of the aforementioned scattering mechanisms to spin-dephasing time in the presence of DP effect were examined by solving the equations numerically. Spin-dephasing time was obtained from the temporal evolution of the incoherently summed spin coherence. Effects of temperature, impurity level, magnetic field, and electron density on spin-dephasing time were investigated. Spin-dephasing time was found to increase with increasing magnetic field. Contrary to predictions of previous simplified treatments of the DP effect, spin-dephasing time was found to increase with temperature in the presence of impurity scattering. These results were found to agree qualitatively with results of recent experiments.

This work was done by C. Z. Ning of **Ames Research Center** *and M. W. Wu of the University of California. Further information is contained in a TSP (see page 1).*

Inquiries concerning rights for the commercial use of this invention should be addressed to the Patent Counsel, Ames Research Center, (650) 604-5104. Refer to ARC-15067-1.

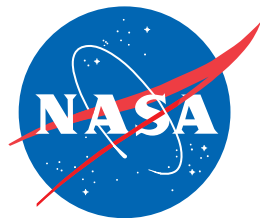## Update on Area Production in Mixing of Supercritical Fluids

The paper "Turbulence and Area Production in Binary-Species, Supercritical Transitional Mixing Layers" presents a more recent account of the research summarized at an earlier stage in "Area Production in Supercritical, Transitional Mixing Layers" (NPO-30425), *NASA Tech Briefs*, Vol. 26, No. 5 (May 2002) page 79. The focus of this research is on supercritical C_7H_{16}/N_2 and O_2/H_2 mixing layers undergoing transitions to turbulence. The C_7H_{16}/N_2 system serves as a simplified model of hydrocarbon/air systems in gas-turbine and diesel engines; the O_2/H_2 system is representative of liquid rocket engines. One goal of this research is to identify ways of controlling area production to increase disintegration of fluids and enhance combustion in such engines. As used in this research, "area production" signifies the fractional rate of change of surface area oriented perpendicular to the mass-fraction gradient of a mixing layer. In the study, a database of transitional states obtained from direct numerical simulations of the aforementioned mixing layers was analyzed to investigate global layer characteristics, phenomena in regions of high density-gradient magnitude (HDGM), irreversible entropy production and its relationship to the HDGM regions, and mechanisms leading to area production.

This work was done by Nora Okong'o and Josette Bellan of Caltech for **NASA's Jet Propulsion Laboratory**. *Further information is contained in a TSP (see page 1). NPO-40030*

Quasi-Sun-Pointing of Spacecraft Using Radiation Pressure

A report proposes a method of utilizing solar-radiation pressure to keep the axis of rotation of a small spin-stabilized spacecraft pointed approximately (typically, within an angle of 10° to 20°) toward the Sun. Axisymmetry is not required. Simple tilted planar vanes would be attached to the outer surface of the body, so that the resulting spacecraft would vaguely resemble a rotary fan, windmill, or propeller. The vanes would be painted black for absorption of Solar radiation. A theoretical analysis based on principles of geometric optics and mechanics has shown that torques produced by Solar-radiation pressure would cause the axis of rotation to precess toward Sun-pointing. The required vane size would be a function of the angular momentum of the spacecraft and the maximum acceptable angular deviation from Sun-pointing. The analysis also shows that the torques produced by the vanes would slowly despin the spacecraft — an effect that could be counteracted by adding specularly reflecting "spin-up" vanes.

This work was done by Thomas Spilker of Caltech for **NASA's Jet Propulsion Laboratory**. *Further information is contained in a TSP (see page 1). NPO-40047*

National Aeronautics and
Space Administration